Micro-strain sensing using wrinkled stiff thin films on soft substrates as tunable optical grating

Teng Ma,[1,4] Hanshuang Liang,[2,4] George Chen,[2] Benny Poon,[3] Hanqing Jiang,[1] and Hongbin Yu[2,*]

[1] *School for Engineering of Matter, Transport and Energy, Arizona State University, Tempe, AZ, USA*
[2] *School of Electrical, Computer and Energy Engineering, Arizona State University, Tempe, USA*
[3] *Intel Corporation, 5000 W. Chandler Blvd., Chandler, AZ 85226, USA*
[4] *These authors contributed equally to this work.*
[*] *yuhb@asu.edu*

Abstract: We report a strain sensing approach that utilizes wrinkled patterns on poly (dimethylsiloxane) (PDMS) as an optical grating to measure thermally-induced strain of different materials. The mechanism for the strain sensing and the effect of PDMS grating on strain sensing are discussed. By bonding the PDMS grating onto a copper or silicon substrate, the coefficient of thermal expansion (CTE) of the substrates can be deduced by measuring the diffraction angle change due to the change in PDMS grating periodicity when thermal strain is introduced. The measured CTEs agree well with the known reference values.

OCIS codes: (050.0050) Diffraction and gratings; (220.4000) Microstructure fabrication.

References and links

1. K. Efimenko, M. Rackaitis, E. Manias, A. Vaziri, L. Mahadevan, and J. Genzer, "Nested self-similar wrinkling patterns in skins," Nat. Mater. **4**(4), 293–297 (2005).
2. X. Y. Jiang, S. Takayama, X. P. Qian, E. Ostuni, H. K. Wu, N. Bowden, P. LeDuc, D. E. Ingber, and G. M. Whitesides, "Controlling mammalian cell spreading and cytoskeletal arrangement with conveniently fabricated continuous wavy features on poly(dimethylsiloxane)," Langmuir **18**(8), 3273–3280 (2002).
3. P. Uttayarat, G. K. Toworfe, F. Dietrich, P. I. Lelkes, and R. J. Composto, "Topographic guidance of endothelial cells on silicone surfaces with micro- to nanogrooves: Orientation of actin filaments and focal adhesions," J. Biomed. Mater. Res. A **75A**(3), 668–680 (2005).
4. C. H. Lu, H. Mohwald, and A. Fery, "A lithography-free method for directed colloidal crystal assembly based on wrinkling," Soft Matter **3**(12), 1530–1536 (2007).
5. A. Schweikart and A. Fery, "Controlled wrinkling as a novel method for the fabrication of patterned surfaces," Mikrochim. Acta **165**(3-4), 249–263 (2009).
6. S. Wagner, S. P. Lacour, J. Jones, P.-I. Hsu, J. C. Sturm, T. Li, and Z. Suo, "Electronic skin: architecture and components," Physica E **25**(2-3), 326–334 (2004).
7. S. P. Lacour, S. Wagner, Z. Huang, and Z. Suo, "Stretchable gold conductors on elastomeric substrates," Appl. Phys. Lett. **82**(15), 2404–2406 (2003).
8. S. P. Lacour, J. Jones, Z. Suo, and S. Wagner, "Design and performance of thin metal film interconnects for skin-like electronic circuits," IEEE Electron Device Lett. **25**(4), 179–181 (2004).
9. S. P. Lacour, J. Jones, S. Wagner, T. Li, and Z. Suo, "Stretchable interconnects for elastic electronic surfaces," Proc. IEEE **93**(8), 1459–1467 (2005).
10. S. P. Lacour, S. Wagner, R. J. Narayan, T. Li, and Z. Suo, "Stiff subcircuit islands of diamondlike carbon for stretchable electronics," J. Appl. Phys. **100**(1), 014913 (2006).
11. C. Yu and H. Jiang, "Forming wrinkled stiff films on polymeric substrates at room temperature for stretchable interconnects applications," Thin Solid Films **519**(2), 818–822 (2010).
12. W. M. Choi, J. Song, D.-Y. Khang, H. Jiang, Y. Y. Huang, and J. A. Rogers, "Biaxially stretchable "wavy" silicon nanomembranes," Nano Lett. **7**(6), 1655–1663 (2007).
13. D.-Y. Khang, H. Jiang, Y. Huang, and J. A. Rogers, "A stretchable form of single-crystal silicon for high-performance electronics on rubber substrates," Science **311**(5758), 208–212 (2006).
14. H. Q. Jiang, Y. G. Sun, J. A. Rogers, and Y. G. Huang, "Mechanics of precisely controlled thin film buckling on elastomeric substrate," Appl. Phys. Lett. **90**(13), 133119 (2007).
15. K. M. Choi and J. A. Rogers, "A photocurable poly(dimethylsiloxane) chemistry designed for soft lithographic molding and printing in the nanometer regime," J. Am. Chem. Soc. **125**(14), 4060–4061 (2003).
16. H. Jiang, D.-Y. Khang, J. Song, Y. Sun, Y. Huang, and J. A. Rogers, "Finite deformation mechanics in buckled thin films on compliant supports," Proc. Natl. Acad. Sci. U.S.A. **104**(40), 15607–15612 (2007).

#187996 - $15.00 USD Received 29 Mar 2013; revised 25 Apr 2013; accepted 26 Apr 2013; published 9 May 2013

17. C. Yu, C. Masarapu, J. Rong, B. Wei, and H. Jiang, "Stretchable Supercapacitors Based on Buckled Single-Walled Carbon - Nanotube Macrofilms," Adv. Mater. **21**(47), 4793–4797 (2009).
18. C. Yu, Z. Wang, H. Yu, and H. Jiang, "A stretchable temperature sensor based on elastically buckled thin film devices on elastomeric substrates," Appl. Phys. Lett. **95**(14), 141912 (2009).
19. C. M. Stafford, C. Harrison, K. L. Beers, A. Karim, E. J. Amis, M. R. VanLandingham, H. C. Kim, W. Volksen, R. D. Miller, and E. E. Simonyi, "A buckling-based metrology for measuring the elastic moduli of polymeric thin films," Nat. Mater. **3**(8), 545–550 (2004).
20. J. L. Wilbur, R. J. Jackman, G. M. Whitesides, E. L. Cheung, L. K. Lee, and M. G. Prentiss, "Elastomeric optics," Chem. Mater. **8**(7), 1380–1385 (1996).
21. C. J. Yu, K. O'Brien, Y. H. Zhang, H. B. Yu, and H. Q. Jiang, "Tunable optical gratings based on buckled nanoscale thin films on transparent elastomeric substrates," Appl. Phys. Lett. **96**(4), 041111 (2010).
22. N. Bowden, S. Brittain, A. G. Evans, J. W. Hutchinson, and G. M. Whitesides, "Spontaneous formation of ordered structures in thin films of metals supported on an elastomeric polymer," Nature **393**(6681), 146–149 (1998).
23. N. Bowden, W. T. S. Huck, K. E. Paul, and G. M. Whitesides, "The controlled formation of ordered, sinusoidal structures by plasma oxidation of an elastomeric polymer," Appl. Phys. Lett. **75**(17), 2557–2559 (1999).
24. J. S. Sharp and R. A. Jones, "Micro-buckling as a route towards surface patterning," Adv. Mater. **14**(11), 799 (2002).
25. H. Schmid, H. Wolf, R. Allenspach, H. Riel, S. Karg, B. Michel, and E. Delamarche, "Preparation of metallic films on elastomeric stamps and their application for contact processing and contact printing," Adv. Funct. Mater. **13**(2), 145–153 (2003).
26. A. U. Manual, "Version 6.5, Hibbitt, Karlsson and Sorensen," Inc., Pawtucket, RI (2004).
27. R. Li, Y. Li, C. Lü, J. Song, R. Saeidpouraza, B. Fang, Y. Zhong, P. M. Ferreira, J. A. Rogers, and Y. Huang, "Thermo-mechanical modeling of laser-driven non-contact transfer printing: two-dimensional analysis," Soft Matter **8**(27), 7122–7127 (2012).
28. C. S. Selvanayagam, J. H. Lau, X. Zhang, S. Seah, K. Vaidyanathan, and T. Chai, "Nonlinear thermal stress/strain analyses of copper filled TSV (through silicon via) and their flip-chip microbumps," IEEE Trans. Adv. Pack. **32**(4), 720–728 (2009).
29. B. H. Jo, L. M. Van Lerberghe, K. M. Motsegood, and D. J. Beebe, "Three-dimensional micro-channel fabrication in polydimethylsiloxane (PDMS) elastomer," J. Microelectromech. Syst. **9**(1), 76–81 (2000).

1. Introduction

Wrinkling (or buckling) is a commonly observed mechanical instability phenomenon typically treated as a nuisance. In recent years, researchers have proposed the use of ordered wrinkling structures of stiff thin films on soft substrates with wavelengths in the nanometer to micrometer order, in a broad spectrum of applications, such as, microfluidic devices [1], templates for cell guidance [2, 3] and colloidal particles assembly [4, 5], stretchable electronic interconnects [6–11], stretchable electronic devices [12–18], modern metrology methods [19], tunable diffraction and phase gratings [1, 2, 20, 21], and methods for micro/nano-fabrication [22–25].

Currently, diffraction gratings are conventionally manufactured using two methods. The first method is the use of ruling engines in a diamond turning technique, where a high precision stage equipped with diamond tips is used in the manufacturing process. This method however, is a serial process, and is typically slow and expensive. The second method utilizes laser technology. Diffraction gratings made this way are called holographic gratings and have sinusoidal grooves. They are rigid and not tunable.

In this paper, we report a novel grating manufacturing technique by using buckled thin stiff film on soft substrates as a grating, which has distinct advantages over the two methods mentioned above. The proposed technique employs the use of a much simpler manufacturing process which only involves a mechanical straining process on soft substrates (e.g., polydimethylsiloxane (PDMS)), an oxygen plasma treatment step, and a routine metal (e.g., Au) deposition step. The simplicity of the fabrication steps allows the proposed technique to have significant cost advantage over conventional methods.

Here PDMS/Au gratings are utilized as tunable strain sensors. A PDMS/Au grating is first attached to the specimen of interest. Any change to the strain of the specimen (thermally or mechanically induced) is imparted to the grating and changes its periodicity. The strain sensing mechanism relies on the detection of the variation in the diffraction angle of the laser beam shinning on the surface of the tunable grating. The variation in diffraction angle can then be related to the strain induced by the specimen of interest. The proposed tunable strain

#187996 - $15.00 USD Received 29 Mar 2013; revised 25 Apr 2013; accepted 26 Apr 2013; published 9 May 2013

sensor and its detection mechanism are expected to have high strain sensitivity in capturing the strain variations within specimen.

2. Fabrication of PDMS/Au grating

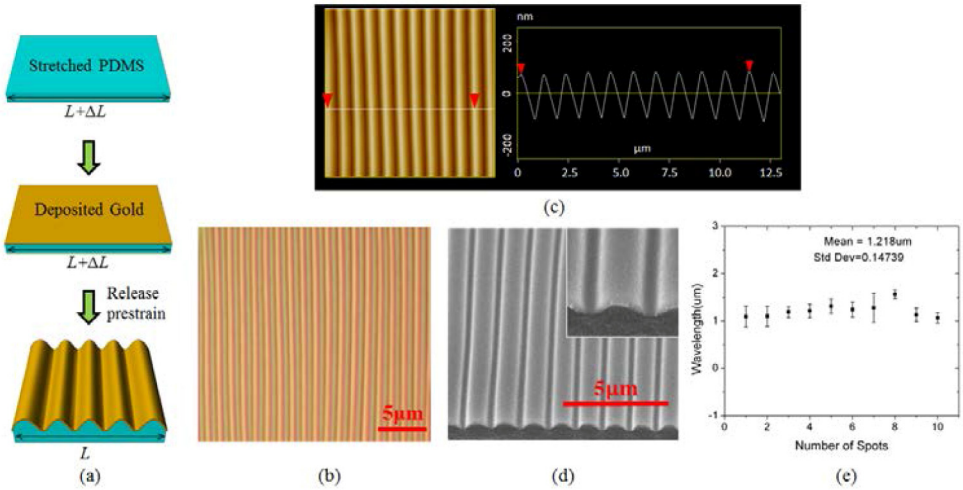

Fig. 1. (a) Schematic of the fabrication process for PDMS/Au grating. (b) Optical microscopy image and (c) AFM image of wrinkling profile of PDMS/Au grating surface. (d) SEM image of wrinkles. (e) Wrinkling wavelength (period) distribution at ten different spots over a surface area of 100 × 100 μm^2. The wrinkling period remains largely constant over this surface area, in good agreement with the calculated period value by Eq. (1). The error bars are one standard deviation of the data, which is taken as the experimental uncertainty of the measurement.

Figure 1(a) illustrates the fabrication flow of the PDMS/Au grating. A polydimethylsiloxane (PDMS) elastomer (Sylgard 184, Dow Corning) was made by mixing the base component and the curing agent in a 10:1 ratio by weight, followed by de-gassing and curing at 80°C for 3 hours. A slab of PDMS elastomer (0.1-1 mm thick) was mounted and elastically stretched by a home-made stage with designed uniaxial pre-strain. After being exposed to oxygen plasma (50 W) for 1 minute to enhance the adhesion, the pre-strained PDMS slab was sputter-coated with a gold (90%)/palladium (10%) (Au/Pd) alloy film of nanoscale thickness. The addition of palladium to gold increases its bonding strength, known as white gold. Due to the small proportion of palladium we will refer to the alloy as gold. Finally, the relaxation of the pre-strain in the PDMS substrates compresses the Au thin film, leading to the deformation and wrinkling in both the Au film and PDMS substrate surface in a sinusoidal pattern. This is a result of the minimization of the system's potential energy by the out-of-plane deformation. The wrinkling period, d, is determined by the mechanical properties of Au film and PDMS substrate, the pre-strain ε_{pre}, and the thickness of the gold film, as described previously [21]

$$d = \frac{2\pi h_f}{\left(1+\varepsilon_{pre}\right)\left[1+\frac{5}{32}\varepsilon_{pre}\left(1+\varepsilon_{pre}\right)\right]^{1/3}}\left[\frac{E_f\left(1-\nu_s^2\right)}{3E_s\left(1-\nu_f^2\right)}\right]^{1/3}. \qquad (1)$$

where h_f is the thickness of the Au film, E is Young's modulus and ν is Poisson's ratio. The subscripts "s" and "f" refer to the PDMS substrate and Au film, respectively. By varying the pre-strain ε_{pre} and the Au film thickness h_f, the buckling period d can be tuned with a broad range. In this work, the buckling period is in the order of micron or sub-micron range for the optimal grating efficiency for the visible light, which is employed for strain sensing application as discussed below.

#187996 - $15.00 USD Received 29 Mar 2013; revised 25 Apr 2013; accepted 26 Apr 2013; published 9 May 2013

Figure 1(b) shows an optical microscopy image of a PDMS/Au grating fabricated by the above mentioned method, with h_f = 10 nm, ε_{pre} = 15%, and the measured buckling period d = 1.22 μm, which agrees well with the calculated value of 1.20 μm obtained from Eq. (1) when the following material parameters are used, E_f = 80 GPa, E_s = 2 MPa, h_f = 10 nm,ν ν_f = 0.3, and ν_s = 0.4921. Figure 1(c) shows the atomic force microscopy (AFM) image of the grating topography and a line-scan profile, which illustrates the uniformity of the buckling in a small area. Figure 1(d) illustrates scanning electron microscopy (SEM) image of the continuous gold film along wave direction on PDMS. To examine the uniformity over a large area, the buckling periods were measured at ten different locations on an area of 100 × 100 μm^2 and the results are shown in Fig. 1(e). It was found that the buckling period is uniform over a large area.

3. Optical setup for micro-strain sensing

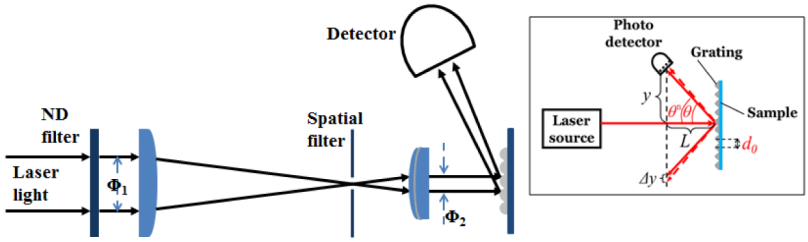

Fig. 2. Optical setup for micro-strain measurement.

A highly sensitive optical diffraction approach was developed to measure strain on the specimen of interest. By using a PDMS/Au grating attached to different specimens (for example, a silicon substrate), a minuscule change in strain within the specimen can be detected with a large change in displacement measured by the photo detector. This mechanism starts from the simple diffraction equation, $d_0\sin\theta = m\lambda$, which relates the diffraction angle θ, initial grating period d_0, and laser source wavelength λ, m is the order of diffraction, when laser beam is normal to the grating surface. As shown in the inset of Fig. 2, the optical setup for strain measurement, a geometric relation, $\tan\theta = y/L$, relates the horizontal position L of the specimen and vertical position y of the photo detector.

When a strain is induced on the specimen through either mechanical or thermal means, the grating period changes from d_0 to d (= d_0 + Δd) and leads to the change in diffraction angle θ by $\Delta\theta$. Meanwhile, the change of θ results in the change of y by Δy, which linearly depends on Δd, as shown below,

$$\Delta y = -\frac{\lambda L}{d_0^2\left(1-\frac{m^2\lambda^2}{d_0^2}\right)^{3/2}}\Delta d = -\frac{\lambda L}{d_0\left(1-\frac{m^2\lambda^2}{d_0^2}\right)^{3/2}}\varepsilon = -A\,\varepsilon. \qquad (2)$$

where the strain ($\varepsilon = \Delta d / d_0$) of the specimen is related to Δy by the pre-factor A.

When L is in the order of 10 cm, and the buckling period d_0 and light wavelength λ, both in the order of sub-micron ($m\lambda < d_0$), the magnification factor A is approximately 1 × 10^7 μm. To put this in perspective, one micro-strain (10^{-6}) leads to a 10 μm change in the vertical position y of the photo detector, which is significantly easier to be measured. In addition, this magnification factor, A, can be further amplified by properly choosing a d_0 that approaches λ (Eq. (2)). This simple mechanism of magnification forms the basis of this highly sensitive strain measurement technique.

Figure 2 illustrates the optical setup used in the micro-strain sensing. The light source was a 633 nm He-Ne laser with output power of 21 mW. The laser spot size had been reduced

#187996 - $15.00 USD Received 29 Mar 2013; revised 25 Apr 2013; accepted 26 Apr 2013; published 9 May 2013

from 700 μm (Φ_1) to 200 μm (Φ_2) in diameter at the grating surface through the use of two optical lenses. In order to improve the signal to noise ratio, an optical chopper was placed before the series of optical lenses to synchronize with the optical detector. A 50/50 beam splitter generated a reference light signal which was fed into an auto-balanced photo detector. The photo detector compared the first order diffracted beam from the grating with the reference light to improve the signal-to-noise ratio for high sensitivity.

4. Results and discussion

PDMS effect: The change in measured diffraction angle directly relates to the change in periodicity of the PDMS/Au grating: One glaring question that needs to answered is whether or not the strain on the grating reflects the underlying strain on the specimen of interest. The commerical finite element package ABAQUS [26] was used to study this effect. Figure 3(a) shows the model, including a PDMS grating with a thickness of 100 μm and length L on top of a 0.5 mm thick, 10 mm long silicon substrate. Thermal stress analysis is conducted by introducing a uniform temperature change ΔT. The PDMS and silicon substrate are modeled by 4-node plane strain temperature-displacement coupled elements (CPE4T). The PDMS-Si interface is treated as shared nodes. The bottom of the silicon substrate is confined. The top Au layer is not considered in the finite element analysis because its thickness is negligible (10 nm). The following material parameters are used in the analysis [27]: E_{PDMS} = 2 MPa, ν_{PDMS} = 0.5, $\alpha_{PDMS} = 310 \times 10^{-6}$ /°C, E_{Si} = 130 GPa, ν_{Si} = 0.3, $\alpha_{Si} = 2.6 \times 10^{-6}$ /°C, ΔT = 50°C, where α is the coefficient of thermal expansion (CTE).

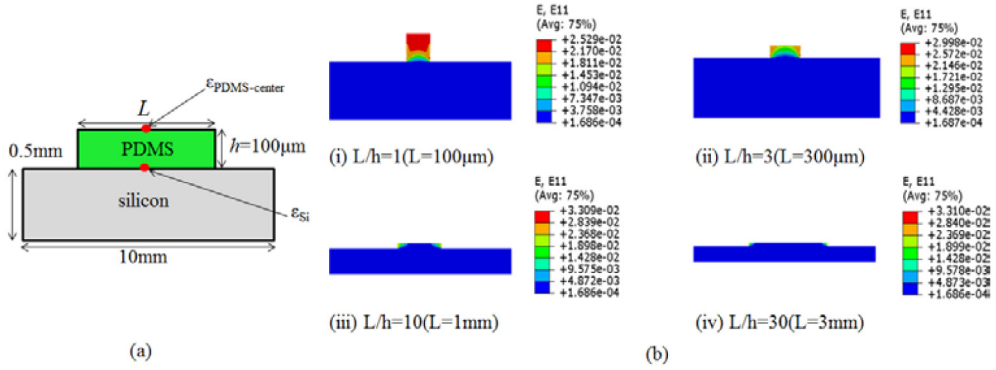

Fig. 3. (a) Schematic of PDMS grating attached on silicon substrate. (b) Strain contours in the horizontal direction for different ratios of PDMS lengths (L) and a constant thickness (h = 100 μm).

Strain contours in the horizontal direction for different ratios of PDMS length and thickness are shown in Fig. 3(b). For L/h = 1, the strain at the top surface of the center of the PDMS (ε_{PDMS}) is about two order of magnitude higher than the strain at the top of the silicon substrate (ε_{Si}). The explanation for this is that for a small L/h ratio, the constraint from the underlying silicon substrate is too weak. Therefore, the strain at the top of the PDMS grating, in this case, only reflects the PDMS itself and not the underlying silicon. As the L/h ratio increases, the constraint from the silicon substrate is increased and the strain at the top of the PDMS grating begins to resemble more and more like the strain of underlying silicon specimen of interest, as can be seen in Fig. 3(b). For an L/h ratio of 30, the strain of the PDMS grating is equal to the strain of the underlying silicon specimen of interest over 80% of the entire surface area of the PDMS grating. In this scenario, the detected strain ε_{PDMS} reflects the actual strain ε_{Si}.

Figure 4(a) shows the ratio of ε_{PDMS} and ε_{Si} as a function of L/h ratio for PDMS grating on Si substrate. It can be seen that when the L/h ratio exceeds a critical value of 20, the ε_{PDMS} reflects ε_{Si} with only a 5% error. Figure 4(b) shows that this relation (i.e., $L/h > 20$) holds for

#187996 - $15.00 USD Received 29 Mar 2013; revised 25 Apr 2013; accepted 26 Apr 2013; published 9 May 2013

all temperature change due to the linearity of this relation. In fact, this analysis is likely to provide an upper bound of the *L*/*h* ratio because the CTE mismatch between silicon and PDMS is likely to be more severe than most conventional metals and polymers. However, note that for materials with a smaller CTE than silicon, such as, glass and other low CTE ceramics, the critical value for *L*/*h* ratio can be smaller than 20.

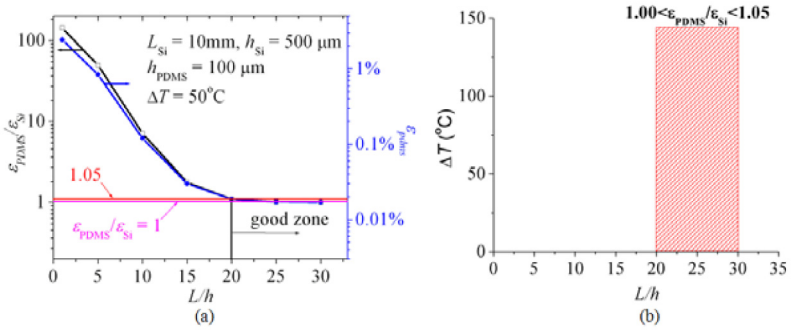

Fig. 4. (a) $\varepsilon_{pdms}/\varepsilon_{Si}$ and ε_{pdms} as a function of L/h. (b) Phase diagram of $\varepsilon_{pdms}/\varepsilon_{Si}$.

Simulation on diffracted laser beam intensity variation: Although the proposed method for strain measurement seems simple (Fig. 2), it is important to consider whether or not the shift in the peak position of the diffraction light due to a small strain can be differentiated. The laser spot size is an important parameter to consider. Figure 5(a) shows the simulation model with a *N*-slit grating, where *N* is the number of slits with periodicity *d* (= *a* + *b*) for each slit. In other words, it is assumed that the laser light is shone on these *N* slits with a spot size of *Nd*. Within each slit, the opening and blocking region sizes are *a* and *b*, respectively. The detector is modeled as a screen. It is assumed that the light is incident and normal to the slits with a fixed ratio of *d*/*a*. The superposition of the waves from all the points within a single slit at point *P*, on the screen has an expression of,

$$U_1 = \int du_1 = \int_0^a \frac{A_0}{a} e^{-i\omega t} e^{ikx\sin\theta} dx\,, \tag{3}$$

where A_0 is the amplitude of the waves, $k = 2\pi/\lambda$ is the wave number of the incident light. The integration is over the opening area of the single slit.

At point *P*, the contribution from all *N* slits is expressed as the summation over all these *N* slits,

$$U = A_0 \frac{\sin\alpha}{\alpha} \frac{\sin N\beta}{\beta} \exp\left\{ i \frac{\left[a + (N-1)\right]\sin\theta}{\lambda} \omega t \right\}, \tag{4}$$

where $\alpha = (\pi a/\lambda)\sin\theta$, $\beta = (\pi d/\lambda)\sin\theta$.

Thus, the light intensity profile at point *P* is given by

$$I_P = U^2 = I_0 \left(\frac{\sin\alpha}{\alpha} \right)^2 \left(\frac{\sin N\beta}{\beta} \right)^2. \tag{5}$$

where $I_0 = A_0^2$ is the intensity of light impinging on the diffraction grating.

#187996 - $15.00 USD Received 29 Mar 2013; revised 25 Apr 2013; accepted 26 Apr 2013; published 9 May 2013

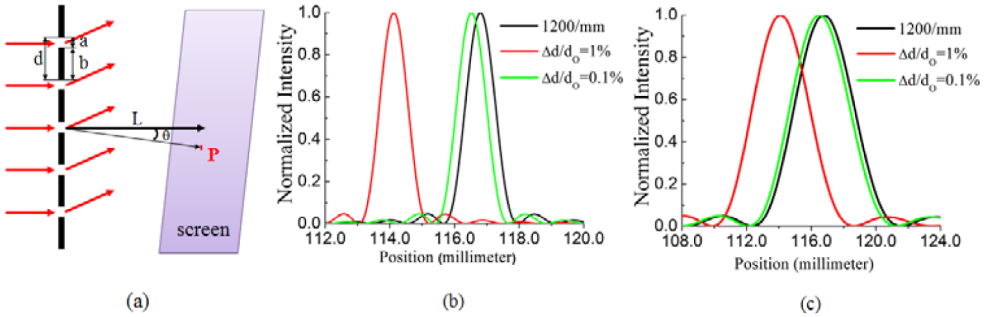

Fig. 5. Diffracted beam intensity simulations based on the multi-slit grating model shown in (a), with grating to screen distance L = 10 cm. Small variations are applied to the grating periodicity to obtain the peak shift, as illustrated in (b) and (c). Spot size is 200 μm (or number of slits N = 240) in (b), and 50 μm (or N = 60) in (c).

Figure 5(b) shows the first order diffraction patterns with a laser spot size of 200 μm and grating to screen distance L = 10 cm. The black line indicates the measurement when no strain is applied, while the red and green lines represent intensity profile when 1% and 0.1% strain applied, respectively. In this case, the laser wavelength is set to be 633 nm, the number of slits N is set to be 240, and the initial grating period is 833.3 nm (i.e., 1,200 lines/mm). Figure 5(c) shows the same results as Fig. 5(b) but with a 50 μm laser spot size. It is clear that a smaller grating period variation leads to a smaller peak shift. This comparison suggests that a detector with high sensitivity is required to capture the localized strain variation with a very small laser spot size. Quantitative analysis indicating further reducing laser spot size to 10 μm and with N = 12 for d = 800 nm grating, a 0.1% strain will lead to light intensity change on the order of 10^{-4}, well within the limit of the auto-balanced photo detector chosen in the experiment. The strain sensitivity in our detection scheme can be estimated. The auto-balanced photodetector used in our experiment can detect optical intensity variation on the order of 10^{-6}, therefore 1 nW intensity difference for 1 mW signal due to diffraction peak shift can be translated to a strain of 2.3 x 10^{-6} for a laser spot size of 200 μm from simulation and through Eq. (2).

Benchmark of strain measurement: To verify the micro-strain sensing technique with tunable PDMS/Au grating proposed earlier, thermal strains of various materials, with differing coefficient-of-thermal-expansions (CTE) spanning 3 orders of magnitude were measured. PDMS/Au gratings are bonded on specimens that are heated up by a copper block, as shown in Fig. 6. A thermal couple is attached to the copper block to form a feedback system for the temperature control. In this system, the temperature reading on the specimen is calibrated to be within one degree of accuracy, and the temperature range for the strain measurement is between room temperature and 65 °C. The laser spot size is 200 μm.

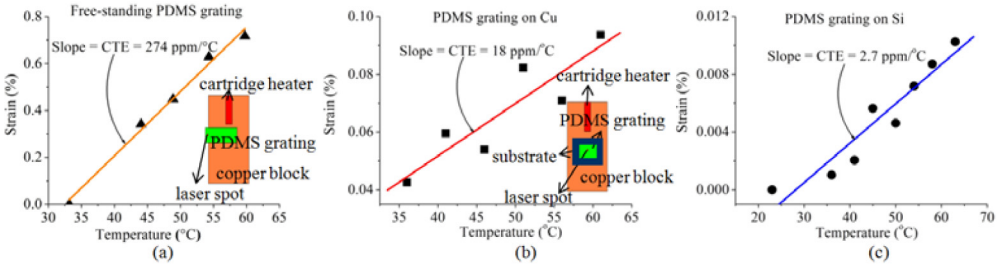

Fig. 6. Measured CTE results for (a) freestanding PDMS, (b) Cu and (c) Si. Insets are the schematics of the setup for thermal micro-strain measurement.

The first specimen is a freestanding PDMS grating, which is hanging over at the edge of the copper block, as shown in the inset schematic in Fig. 6(a). The focused laser spot is

#187996 - $15.00 USD Received 29 Mar 2013; revised 25 Apr 2013; accepted 26 Apr 2013; published 9 May 2013

located just off the copper block to measure the thermal strain of the PDMS grating without constraints from the copper block. Figure 6(a) shows the measured strain as a function of temperature for this freestanding PDMS grating, where a good linearity is observed. The CTE of PDMS, i.e., the slope of strain/temperature relation, is 274 ppm/°C (part per million per degree Celsius), which agrees with the reference value of the CTE of PDMS, 265 ppm/°C, measured using commercial thermal-mechanical analysis tool Q400 from TA instruments, under expansion mode at 10 mN force.

The second specimen is a piece of copper sheet, on which the PDMS/Au grating is attached by a thin double-sided adhesive tape. The size of PDMS/Au grating has been chosen based on Fig. 4(a) to ensure the measured strain on top of the grating accurately reflects the strain of copper substrate. Figure 6(b) shows the strain-temperature relation. The CTE of copper given by the slope is obtained as 18.2 ppm/°C, which is consistent with the CTE value of copper (17.5 ppm/°C) [28]. Some of the data points in Fig. 6(b) are scattered compared to Fig. 6(a), which can be attributed to the bonding quality of the adhesive tape between copper and PDMS.

The last specimen is a Si substrate. The PDMS/Au grating can be firmly bonded to the Si substrate by treating the Si surface with oxygen plasma to form a SiO_2 bond between the PDMS and Si [29]. Si has a much lower CTE (2.6 ppm/°C), compared to previous two specimen materials. The experimental data is plotted in Fig. 6(c), which gives an extracted CTE value of 2.73 ppm/°C, very close to the reference value of the Si CTE. The measured data here show much less fluctuation than the data from the PDMS bonded to copper as the result of much better bonding quality between Si and PDMS. The successful measurement of such small strain on Si on the order of 10^{-5}, or a few nanometers displacement within 200 μm laser spot size, demonstrates the high strain sensitivity of this technique as a result of the unique grating fabrication technique and strain detection strategy. The results shown in Fig. 6 are representatives from many measurements we have performed, where several samples on each type of substrate were fabricated and measured, with each sample undergone a repeated temperature increase/decrease cycles, and the results show good repeatability.

5. Conclusions

PDMS tunable gratings fabricated through buckled film were used for micro-strain measurement of various materials. A highly sensitive optical setup optimized to amplify the small strain signal to the change in diffraction angle, orders of magnitude larger, was proposed. The applicability of the PDMS/Au grating to infer the strain of the underlying specimen of interest, require the L/h aspect ratio of the grating to greater than 20 for most practical purposes. In addition, the laser spot size was demonstrated to influence the measurement resolution significantly. Lastly, the thermal strain measurement on the free-standing PDMS grating as well as the PDMS grating bonded to copper and Si substrates agree well with the reference CTE values of PDMS, copper and Si, respectively. This technique is relatively simple for very high strain sensitivity measurement, and its potential spatial scanning capability is also expected to complement the application boundaries of other in-plane strain measurement metrologies such as Moire Interferometry or digital image correlation (DIC) methods in terms of maximum strain gradient, and field-of-view of measurement. In addition, unlike conventional in-plane strain sensing metrologies, the proposed technique is expected to work for non-planar surface geometry, as well.

Acknowledgments

We acknowledge the support from Intel Corporation through an ASU Consortium, Connection One, and stimulating discussions with Ravi Mahajan. TM acknowledges the financial support from the China Scholarship Council. GC would like to thank the Fulton Undergraduate Research Initiative (FURI) program at Arizona State University for providing partial funding and United States National Science Foundation funding through REU program. HJ acknowledges the support from NSF under Grant No. CMMI-0700440. HY acknowledges the support from NSF under Grant No. ECCS-0926017.